Hypoxia imaging with [18F]HX4 PET in NSCLC patients

Radiotherapy and Oncology 109 (2013) 58–64

Contents lists available at ScienceDirect

Radiotherapy and Oncology

journal homepage: www.thegreenjournal.com

Hypoxic imaging in lung cancer

Hypoxia imaging with [^{18}F]HX4 PET in NSCLC patients: Defining optimal imaging parameters

Catharina M.L. Zegers [a,*], Wouter van Elmpt [a], Roel Wierts [b], Bart Reymen [a], Hoda Sharifi [a], Michel C. Öllers [a], Frank Hoebers [a], Esther G.C. Troost [a], Rinus Wanders [a], Angela van Baardwijk [a], Boudewijn Brans [b], Jonas Eriksson [c], Bert Windhorst [c], Felix M. Mottaghy [b,d], Dirk De Ruysscher [a,e], Philippe Lambin [a]

[a] Department of Radiation Oncology (MAASTRO), GROW – School for Oncology and Developmental Biology; [b] Department of Nuclear Medicine, Maastricht University Medical Centre; [c] Department of Nuclear Medicine and PET Research, VU University Medical Centre, Amsterdam, The Netherlands; [d] Department of Nuclear Medicine, University Hospital RWTH Aachen, Germany; [e] University Hospitals Leuven/KU Leuven, Belgium

ARTICLE INFO

Article history:
Received 17 May 2013
Received in revised form 16 August 2013
Accepted 17 August 2013
Available online 14 September 2013

Keywords:
NSCLC
Imaging
Hypoxia
PET
HX4

ABSTRACT

Background and purpose: [^{18}F]HX4 is a promising hypoxia PET-tracer. Uptake, spatio-temporal stability and optimal acquisition parameters for [^{18}F]HX4 PET imaging were evaluated in non-small cell lung cancer (NSCLC) patients.

Materials and methods: [^{18}F]HX4 PET/CT images of 15 NSCLC patients were acquired 2 h and 4 h after injection (p.i.). Maximum standardized-uptake-value (SUV_{max}), tumor-to-blood-ratio (TBR_{max}), hypoxic fraction (HF) and contrast-to-noise-ratio (CNR) were determined for all lesions. To evaluate spatio-temporal stability, DICE-similarity and Pearson correlation coefficients were calculated. Optimal acquisition-duration was assessed by comparing 30, 20, 10 and 5 min acquisitions.

Results: Considerable uptake (TBR >1.4) was observed in 18/25 target lesions. TBR_{max} increased significantly from 2 h (1.6 ± 0.3) to 4 h p.i. (2.0 ± 0.6). Uptake patterns at 2 h and 4 h p.i. showed a strong correlation ($R = 0.77 \pm 0.10$) with a DICE similarity coefficient of 0.69 ± 0.08 for the 30% highest uptake volume. Reducing acquisition-time resulted in significant changes in SUV_{max} and CNR. TBR_{max} and HF were only affected for scan-times of 5 min.

Conclusions: The majority of NSCLC lesions showed considerable [^{18}F]HX4 uptake. The heterogeneous uptake pattern was stable between 2 h and 4 h p.i. [^{18}F]HX4 PET imaging at 4 h p.i. is superior to 2 h p.i. to reach highest contrast. Acquisition time may be reduced to 10 min without significant effects on TBR_{max} and HF.

 Radiotherapy and Oncology 109 (2013) 58–64

Radiotherapy combined with chemotherapy is the standard treatment modality for patients with locally advanced non-small cell lung cancer (NSCLC). Unfortunately, after treatment, progression free survival is short with a median of 14 months [1]. Tumor cell hypoxia is known to be a major factor that negatively influences treatment effectiveness, it promotes resistance to radiotherapy and chemotherapy and increases tumor aggressiveness, angiogenesis, and metastatic potential, resulting in a poor prognosis. [2,3].

Detection and quantification of tumor cell hypoxia using non-invasive positron emission tomography (PET) could help selecting patients who may benefit from treatment adaptation counteracting hypoxia [4,5]. The selective binding and retention of 2-nitroimidazoles allows detection and quantification of tumor hypoxia with PET imaging prior to and during treatment [6–11]. In addition, it provides the opportunity to display the spatial distribution of hypoxia, which is essential for its integration in radiation dose distribution [12]. An increased radiation dose to the radio-resistant/hypoxic areas may result in an increased local control [13–15]. Therefore accurate identification and stable detection of the intra-tumor hypoxic sub-volumes is of importance [16].

Several 2-nitroimidazoles, labeled with fluor-18 [^{18}F], have already been applied in patients to identify hypoxia [17]. The 2-nitroimidazole nucleoside analog: 3-[^{18}F]fluoro-2-(4-((2-nitro-1H-imidazol-1-yl)methyl)-1H-1,2,3-triazol-1-yl)propan-1-ol[^{18}F] HX4, was developed as a potential marker to visualize hypoxic tumor cells [18]. It has a high water solubility and fast clearance from non-hypoxic tissue, therefore generating a tracer with preferred

* Corresponding author. Address: Maastro Clinic, Dr. Tanslaan 12, 6229ET Maastricht, The Netherlands.
E-mail address: karen.zegers@maastro.nl (C.M.L. Zegers).

0167-8140 © 2013 The Authors. Published by Elsevier Ireland Ltd. Open access under CC BY-NC-ND license.
http://dx.doi.org/10.1016/j.radonc.2013.08.031

pharmacokinetic properties [18–20]. Previous preclinical and clinical studies have shown that [^{18}F]HX4 is a promising and non-toxic tracer to visualize tumor hypoxia [18–21]. Imaging data is available at www.cancerdata.org/?q=10.1073/pnas.1102526108 and www.cancerdata.org/?q=10.1007/s00259-010-1437-x. In a rat rhabdomyosarcoma model the [^{18}F]HX4 PET contrast (tumor-to-blood ratio; TBR) increased significantly over time, reaching a plateau and optimal imaging at 4 h after injection [18]. In an inter-patient comparison [^{18}F]HX4 yielded a similar tumor-to-muscle ratio at 1.5 h post-injection (p.i.) than [^{18}F]MISO at 2 h p.i., suggesting that [^{18}F]HX4 may be used with a shorter injection-acquisition time than [^{18}F]MISO [21].

The aims of this study were to evaluate the [^{18}F]HX4 uptake in NSCLC patients, to report spatio-temporal stability, compare imaging at different time-points and evaluate the possibility to reduce acquisition time.

Materials and methods

Patients

Fifteen NSCLC patients analyzed in this study were included in the PET-Boost [15] (NCT01024829) or Nitroglycerin trial (NCT01210378), approved by the appropriate Medical Ethics Review Committee. Written informed consent was obtained from all patients before study entry.

[^{18}F]HX4 PET/CT imaging was acquired at baseline, i.e. before the start of external beam radiotherapy. However, patients were treated with concurrent or sequential chemoradiation and received at least one course of chemotherapy before the start of radiotherapy and [^{18}F]HX4 PET/CT imaging.

PET/CT imaging

Images were acquired on a Philips Gemini TF 64 PET/CT scanner (Philips Healthcare, Best, The Netherlands) with an axial field of view of 18 cm, slice thickness of 4 mm, in plane pixel spacing of 4 mm and a spatial resolution of approximately 5 mm FWHM. CT based attenuation correction and scatter correction (SS-SIMUL) were performed. The PET images were reconstructed using 3D ordered-subset iterative time-of-flight reconstruction technique (BLOB-OS-TF) using 3 iterations and 33 subsets. The patient was scanned in radiotherapy position, positioned on a flat tabletop using a movable laser alignment system with the arms in an arm-support positioned above the head. The field of view for CT and PET imaging was positioned on the primary tumor. [^{18}F]HX4 was produced as described in previous publications [18–21]. The injected activity of [^{18}F]HX4 was 423 ± 72 MBq based on a previous phase I trial [19]. After intravenous administration of [^{18}F]HX4, PET/CT imaging was performed at 2 h and 4 h p.i. A single bed-position PET was acquired with a total acquisition time of 30 min.

Analysis

Gross tumor volumes of the primary tumor (GTV_{prim}) and involved lymph nodes (GTV_{ln}) were defined by an experienced radiation oncologist and evaluated by a second radiation oncologist, on the [^{18}F]fluorodeoxyglucose (FDG) PET/CT scan used for radiotherapy planning purposes, acquired in the same week as the [^{18}F]HX4 PET/CT. [^{18}F]FDG-based GTVs were copied to the [^{18}F]HX4 PET/CT images by rigid registration and a visual check was performed. No matching problems occurred. In addition a volume of interest (VOI) in the aorta was defined as background region.

Scan time point

The optimal imaging time point was evaluated by determining image parameters in the 2 h and 4 h p.i. [^{18}F]HX4 PET scans. The mean and maximum standardized uptake values (SUV_{mean} and SUV_{max}, respectively) in the GTVs and aorta were extracted (PMOD v3.0, Zurich, Switzerland). The tumor-to-background ratio (TBR_{max}) was defined as the ratio of GTV SUV_{max} and aorta SUV_{mean}. The tumor hypoxic fraction (HF) was calculated based on the [^{18}F]HX4 uptake. A threshold for the definition of hypoxia has not been formally established, based on previous publications, a TBR larger than 1.4 was used as the standard threshold to define tumor hypoxia [18,22–24]. In addition, the HF was calculated based on a threshold ranging from TBR >1.1 to TBR >1.6.

Spatio-temporal stability

The spatio-temporal stability was evaluated using two methods, first by calculating the DICE similarity coefficient of the hypoxic volumes and second with a voxel-wise comparison of the [^{18}F]HX4 uptake at 2 h and 4 h p.i. For both methods the CT acquired at 2 h p.i. (CT_{2h}) was rigidly registered to the CT at 4 h p.i. (CT_{4h}). The resulting deformation field was applied to co-register the PET at 2 h p.i. (PET_{2h}) to the PET at 4 h p.i. (PET_{4h}).

To calculate the DICE similarity coefficient; First the percentile of the GTV with the highest uptake on PET_{2h} and PET_{4h} was defined, by using percentiles ranging from 50% to 90%. Second, only for lesions with a HF >5%, the hypoxic volume on the PET_{4h} and its corresponding high uptake volume on the PET_{2h} were defined. The resulting high uptake volumes (UV) are represented by UV_{2h} and UV_{4h}. DICE was calculated using:

$$\mathrm{DICE} = 2\frac{UV_{2h} \cap UV_{4h}}{UV_{2h} + UV_{4h}}$$

Furthermore, a voxel-wise comparison of the [^{18}F]HX4 PET uptake in the GTV in PET_{2h} and PET_{4h} was performed.

Reduced acquisition time

Because hypoxia PET tracers generally have a low uptake in tumors, prolonged PET acquisition times may be preferred. Additional reconstructions were made with reduced acquisition duration. The full acquisition time of 30 min was compared to the first 20, 10 and 5 min acquisitions by evaluating changes in SUV_{max}, TBR_{max}, HF and the contrast-to-noise ratio (CNR) defined as:

$$\mathrm{CNR} = \frac{SUV_{max}\ \text{tumor} - SUV_{mean}\ \text{aorta}}{SUV_{SD}\ \text{aorta}}$$

Statistics

For all parameters mean ± 1 standard deviation (SD) are reported. A Wilcoxon signed rank test was used to determine significant differences in uptake (SUV_{max}, TBR_{max}) between 2 h and 4 h p.i. and to evaluate the effect on image parameters (SUV_{max}, TBR_{max}, HF, CNR) when limiting the acquisition time. Linear regression was performed to correlate SUV_{max} and TBR_{max} from 2 h to 4 h p.i. and to quantify the voxel-wise comparison of the [^{18}F]HX4 uptake within the GTV. Slope and Pearson correlation coefficients were calculated. A p-value smaller than 0.05 was assumed to be statistically significant.

Results

[^{18}F]HX4 PET/CT imaging of 15 NSCLC patients (11 male, 4 female) was included in the analysis. The mean age of the patients was 62 ± 10 years (range 40–82years). Tumor stage ranged from IIB to IV; pathology being adenocarcinoma (n = 8), squamous cell carcinoma (n = 3), large cell carcinoma (n = 3) or not specified (n = 1). All patients were treated with curative intent and had

Table 1
Patient characteristics.

Patient	Age	Gender	TNM	Stage	Pathology	GTV	Size GTV [cm^3]	Prior treatment [no. chemotherapy cycles]
1	55	M	T2aN3M0	IIIB	Large cell carcinoma	prim	48	1
						ln	190	
2	59	F	T4N1M0	IIIB	Adenocarcinoma	prim	328	3
						ln	25	
3	72	M	T2N3M0	IIIB	Adenocarcinoma	prim	42	1
						ln	51	
4	60	M	T4N1M0	IIIB	Adenocarcinoma	prim	859	1
						ln*	8	
5	65	M	T3N2M0	IIIA	Squamous cell carcinoma	prim	148	1
						ln	39	
6	66	M	T2N3M0	IIIB	Unknown	prim	78	1
						ln	13	
7	51	F	T3N2M0	IIIA	Large cell carcinoma	prim	150	2
						ln	11	
8	82	M	T3N0M0	IIB	Adenocarcinoma	prim	63	3
9	66	M	T4N3M0	IIIB	Adenocarcinoma	prim	65	2
						ln[a]	3	
10	62	F	T4N2M0	IIIB	Squamous cell carcinoma	prim	150	1
						ln[a]	5	
11	77	M	T3N2M0	IIIA	Large cell carcinoma	prim	299	1
						ln*	7	
12	64	M	T4N2M0	IIIB	Squamous cell carcinoma	prim	212	1
						ln	13	
13	60	M	T4N2M0	IIIB	Adenocarcinoma	prim	53	2
						ln	17	
14	47	F	T4N3M0	IIIB	Adenocarcinoma	prim	125	1
						ln	204	
15	40	M	T4N2M1	IV	Adenocarcinoma	prim	78	3
						ln	35	

prim = primary lesion, ln = involved lymph nodes.
[a] Lesions with a volume <10 cm^3.

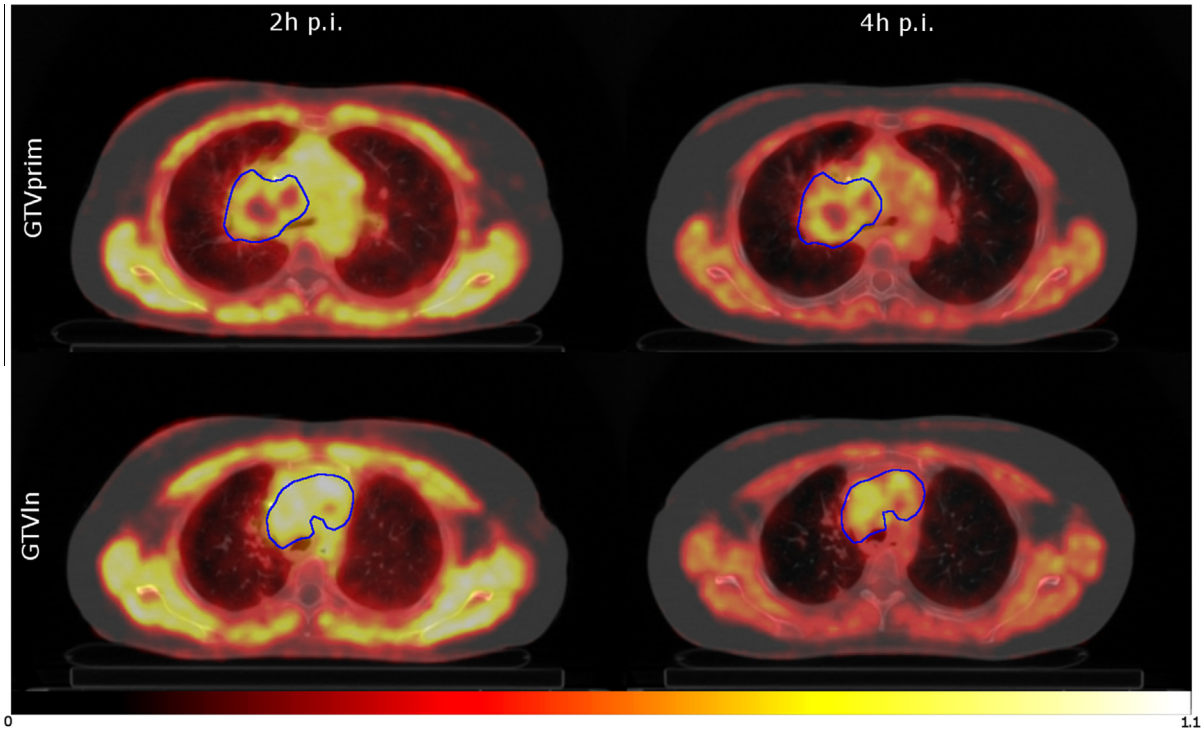

Fig. 1. Example of two transversal slices of the [18F]HX4 CT/PET image of patient 14 at 2 h and 4 h p.i. showing the primary tumor (GTV_{prim}) and involved lymph nodes (GTV_{ln}).

one to three cycles of chemotherapy before hypoxia PET imaging and the start of radiotherapy. Patient characteristics are visualized in Table 1. All but one patient had involvement of the lymph nodes (GTV_{ln}) which were separately analyzed from the primary tumor (GTV_{prim}). Four involved lymph nodes with a volume <10 cm^3 were excluded, due to potential partial volume effects. As a result 25

Table 2
Target lesion characteristics at 2 h and 4 h p.i.

Patient	Lesion	GTV [cm^3]	Tumor SUV$_{max}$		Aorta SUV$_{mean}$		TBR	
			2 h p.i.	4 h p.i.	2 h p.i.	4 h p.i.	2 h p.i.	4 h p.i.
1	prim	48	0.93	0.64	0.88	0.58	1.06	1.10
	ln[c]	190	1.63	1.65			1.87	2.84
2	prim[c]	328	2.19	1.84	0.91	0.53	2.40	3.47
	ln[c]	25	1.63	1.36			1.79	2.56
3	prim[c]	42	0.73[b]	0.65[b]	0.48[b]	0.36[b]	1.51	1.78
	Ln	51	0.63[b]	0.48[b]			1.30	1.33
4	prim[c]	859	0.87[b]	0.85[b]	0.51[b]	0.34[b]	1.71	2.52
	ln[a]	8	0.55[b]	0.44[b]			1.08	1.32
5	prim[c]	148	1.47	1.30	0.98	0.71	1.50	1.83
	ln[c]	39	1.23	1.03			1.26	1.45
6	prim[c]	78	1.49	1.44	0.79	0.62	1.90	2.33
	Ln	13	1.14	0.98			1.45	1.58
7	prim[c]	150	0.91	0.66	0.67	0.44	1.36	1.49
	ln	11	0.73	0.51			1.08	1.15
8	prim[c]	63	1.45	1.63	1.02	0.85	1.43	1.92
	–							
9	prim	65	1.01	0.76	0.85	0.60	1.19	1.26
	ln[a]	3	0.81	0.59			0.95	0.99
10	prim[c]	150	1.28	1.09	0.96	0.62	1.34	1.75
	ln[a,c]	5	1.29	1.24			1.35	2.00
11	prim[c]	299	1.98	1.87	1.18	1.02	1.69	1.83
	ln[a]	7	1.33	1.28			1.13	1.25
12	prim[c]	212	2.03	1.97	1.33	1.06	1.53	1.85
	Ln	13	1.39	1.14			1.04	1.07
13	prim	53	1.00	0.76	0.86	0.56	1.17	1.34
	Ln	17	0.89	0.70			1.04	1.24
14	prim[c]	125	1.12	1.02	0.81	0.54	1.37	1.90
	ln[c]	204	1.19	1.28			1.46	2.37
15	prim[c]	78	1.40	1.13	1.10	0.78	1.27	1.45
	ln[c]	35	1.32	1.19			1.20	1.52
Average [>10 cm^2]		132 ± 175	1.34 ± 0.39	1.18 ± 0.43	0.95 ± 0.18	0.69 ± 0.19	1.44 ± 0.32	1.80 ± 0.60
Average [hypoxic >10 cm^2]		169 ± 195	1.47 ± 0.36	1.34 ± 0.37			1.56 ± 0.30	2.03 ± 0.55

[a] Lesions <10 cm^2.
[b] No absolute SUV.
[c] Hypoxic lesions.

target lesions (GTV$_{prim}$ n = 15, GTV$_{ln}$ n = 10) were selected for analysis, with an average lesion size of 180 ± 208 cm^3 (range 42–859 cm^3) for primary tumor and 60 ± 74 cm^3 (range 11–204 cm^3) for the sum of the pathological lymph nodes.

For two patients (P3 and P4) the SUV values could not be determined due to an undefined amount of residual activity in the administration system. For these patients, absolute SUV was calculated based on the estimated activity in the syringe before injection, but excluded from statistical analysis. TBR$_{max}$, HF and CNR calculations were not affected by this spill and therefore included in the analysis.

Tumor hypoxia, defined as TBR$_{max}$ >1.4 on the 4 h p.i. acquisition, was observed in 80% (12/15) of the primary tumors and 60% (6/10) of lymph node regions. An example of a 2 h and 4 h p.i. PET/CT image is shown in Fig. 1. Comparing 2 h with 4 h p.i., there was a high correlation for both SUV$_{max}$ (R = 0.96) and TBR$_{max}$ (R = 0.94).

Within the hypoxic lesions, the tumor SUV$_{max}$ decreased between 2 h p.i. and 4 h p.i. for both GTV$_{prim}$ (1.5 ± 0.4 to 1.4 ± 0.4; P < 0.001) and GTV$_{ln}$ (1.4 ± 0.2 to 1.2 ± 0.2; P = 0.16). However, due to clearance of [^{18}F]HX4 in the blood, the TBR$_{max}$ increased significantly from 2 h to 4 h p.i. (GTV$_{prim}$: 1.6 ± 0.3 to 2.0 ± 0.6; P < 0.001 and GTV$_{ln}$: 1.5 ± 0.3 to 2.1 ± 0.6; P = 0.03) as shown in Table 2 and Fig. 2. The SUV$_{mean}$ measured within the aorta VOI was 1.0 ± 0.2 and 0.7 ± 0.2 at 2 h p.i. and 4 h p.i., respectively. Assuming an exponential clearance of HX4 in the blood, this resulted in an estimated biological half life of 4.3 h.

The average HF (TBR >1.4), based on the 4 h p.i. image, was 15 ± 19% (GTV$_{prim}$, range 0.1–66%) and 12 ± 13% (GTV$_{ln}$, range

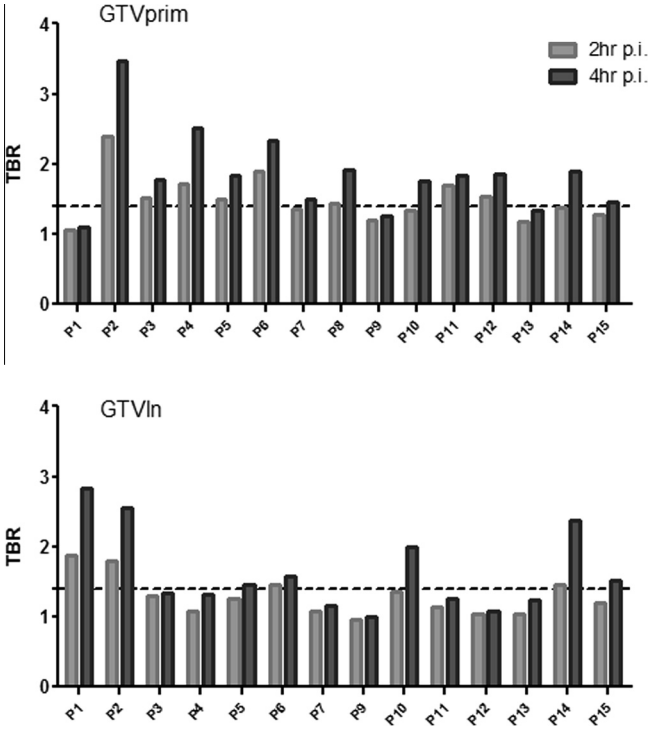

Fig. 2. TBR$_{max}$ of the primary tumor (GTV$_{prim}$) and involved lymph nodes (GTV$_{ln}$) of all patients.

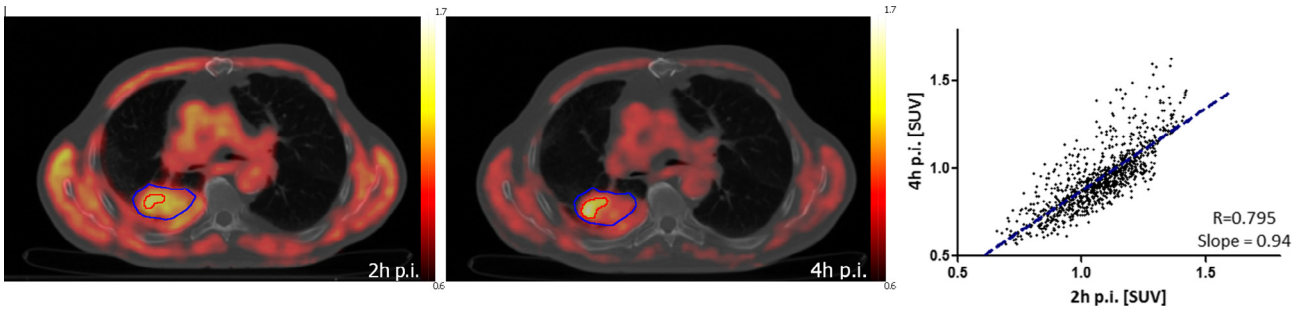

Fig. 3. Example of patient 8. Left figure shows the 2 h p.i. [18F]HX4 PET/CT that is rigidly registered to the 4 h p.i. scan (middle). Visualized are the gross tumor volume (blue) and the hypoxic volume in the 4 h p.i. scan and its corresponding high uptake volume in the 2 h p.i. scan (red). The right figure shows the voxel-wise comparison between 2 h and 4 h p.i. within the gross tumor volume.

0.3–36%) for the hypoxic lesions. No correlation between the GTV and HF was observed ($R = 0.12$, $P = 0.57$). When applying the same threshold (TBR >1.4) in the 2 h p.i. images, a lower amount of hypoxic lesions were detected (8/15 GTV_{prim} and 4/10 GTV_{ln}) and the average HF was reduced to 5 ± 10% (GTV_{prim}) and 3 ± 6% (GTV_{ln}). Using a threshold of TBR >1.2 resulted in a similar hypoxic lesion detection rate (12/15 and 7/10, respectively) and HF (GTV_{prim} 17 ± 17% and GTV_{ln} 10 ± 10%) compared to 4 h p.i., however the use of this lower threshold resulted in one false positive case. The hypoxic fractions based on thresholds ranging from TBR >1.1 to TBR >1.6 on both 2 h and 4 h p.i. acquisitions are summarized in Table S1.

Although the hypoxic lesions showed a heterogeneous [18F]HX4 uptake pattern, the voxel-wise comparison of the PET_{2h} and PET_{4h} showed a strong correlation ($R = 0.77 \pm 0.10$, range: 0.58–0.94, slope: 0.72 ± 0.15), see Fig. 3 and Table S2. Comparing high uptake percentiles resulted in an average DICE similarity coefficient of 0.79 ± 0.06, 0.75 ± 0.06, 0.70 ± 0.08, 0.61 ± 0.10 and 0.48 ± 0.10 for the highest volume percentiles 50%, 60%, 70%, 80% and 90%, respectively. Comparing the hypoxic volumes defined on the PET_{4h} with the corresponding high uptake volume on the PET_{2h} provides a DICE similarity coefficient of 0.61 ± 0.19 (Table S2).

One patient was excluded from this analysis due to an incomplete 30 min acquisition, resulting in 16 evaluable hypoxic lesions (>10 cm^3). Reducing acquisition time from 30 min to the first 20, 10 and 5 min of the acquisition resulted in an average increase in SUV_{max} of 4 ± 6% ($P = 0.014$), 12 ± 15% ($P < 0.001$) and 18 ± 16% ($P = 0.025$). TBR_{max} increased with 2 ± 5% ($P = 0.171$), 7 ± 12% ($P = 0.074$) and 16 ± 13% ($P < 0.001$) for, respectively, the 20, 10 and 5 min acquisition, hence only a significant difference was reached for the 5 min acquisition. The average HF was not significantly different for the 30 min (11 ± 16%), 20 min (11 ± 16%) and 10 min (11 ± 15%) acquisition, again for the 5 min acquisition (average HF: 13 ± 15%) the change in HF was significant ($P = 0.02$). The CNR decreased from 9.5 ± 4.1 (30 min) to 8.7 ± 4.2 (20 min; $P = 0.02$), 7.8 ± 4.7 (10 min; $P < 0.01$) and 6.6 ± 3.2 (5 min; $P < 0.001$). Images of an example patient are visualized in Fig. 4.

Discussion

The aims of this study were to evaluate [18F]HX4 uptake in NSCLC, report spatio-temporal stability, compare imaging at different time-points and evaluate the possibility to reduce acquisition time. Based on this, we want to generate recommendations for future PET imaging with [18F]HX4. [18F]HX4 was developed to provide a hypoxia PET tracer with preferred pharmacokinetic and clearance properties compared to other available nitroimidazoles. Based on the current population the biological half-life of HX4 in the blood is approximately 4.3 h. Which is a 3-fold faster clearance in comparison to [18F]MISO, reported to have a biological half life of 12–13 h [25,26]. In a clinical trial, it was shown that [18F]HX4 provides the same image contrast as [18F]MISO at an earlier time-point after injection [21], a characteristic beneficial for practical reasons. However, previous preclinical and clinical studies have also shown that for both FMISO [6,27] and HX4 [18,19] the later scan time-points are optimal in order to reach a higher image contrast. In the current study the image contrast (TBR_{max}) increased from 2 h to 4 h p.i. confirming the pre-clinical results, i.e. [18F]HX4 scanning at 4 h p.i. provides a better opportunity to identify hypoxic areas. In preclinical setting a TBR plateau was reached at 4 h p.i., however it is still unknown if in the clinical situation, hypoxia imaging at a timepoint later than 4 h p.i. could provide an enhanced image contrast [18].

In literature no evaluation has been performed comparing all hypoxia PET tracers in the same tumor model or patient population [17]. Hence, it is difficult to compare the current results to clinical trials with other hypoxia tracers used in NSCLC imaging. Other studies allowed different treatment modalities before imaging, with differences in scan time p.i. or definition of background tissue (muscle [7], mediastinum [6,28], venous blood sampling [22,29], lung [30], heart [31], not specified [32]). Nevertheless it seems that

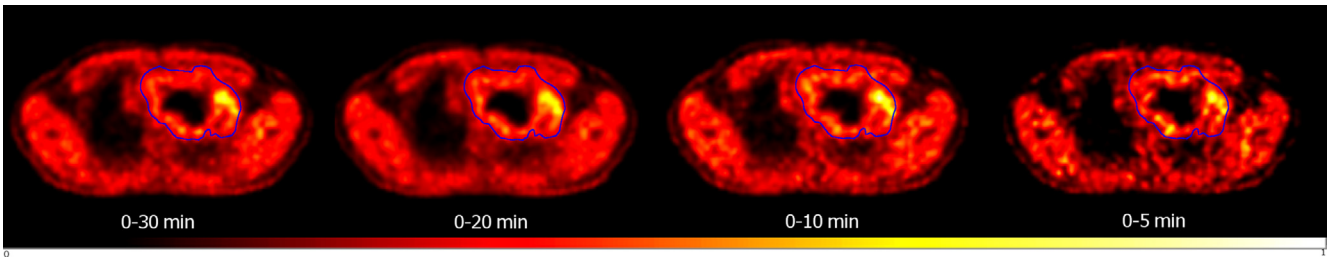

Fig. 4. Transversal [18F]HX4 PET slice of patient 4 at 4 h p.i., reconstructed with the total acquisition of 30 min or the first 20, 10 and 5 min.

the average SUV_{max} resulting from the current analysis are similar compared to other trials with [^{18}F]FMISO [6–8,30], FAZA [32] or FETNIM [29].

The definition of the hypoxic volume in the literature is diverse and based on different tracers. For [^{18}F]FMISO imaging, a comparison with immunohistochemistry [24], normal tissue differences [22] and in vivo bio-distribution data [23] a threshold of TBR >1.4 can be supported. For [^{18}F]HX4 imaging a good correlation with immunohistochemistry was observed when HX4 positive voxels (TBR >1.4) were compared to pimonidazole staining [18], however the optimal TBR in a clinical setting is still under investigation. Using the TBR >1.4 threshold a significant amount of tumor hypoxia was observed in 80% of the primary tumors and 60% of the involved lymph nodes. Note that although the lesion size of GTV_{ln} was in general smaller than GTV_{prim}, still no relationship was found between GTV and HF. An average HF of 14 ± 17% was observed, which is lower in comparison to a previous study of Rasey et al. [22] where a median HF of 58% was reported. The discrepancy might be explained due to the fact that all patients in the current study had at least one cycle of chemotherapy before [^{18}F]HX4 PET scans, which may reduce tumor hypoxia [9,33], resulting in a lower SUV_{max}, TBR and HF. Note that, this is a situation frequently occurring in clinical practice. However, the hypoxic status of the lesion was assessed before the start of radiotherapy, which is of utmost importance in dose redistribution strategies.

The TBR threshold of 1.4 should not be interpreted as a rigid value to determine tumor hypoxia. Due to tracer kinetics, the threshold should be optimized based on scan time post-injection. An alternative threshold of TBR >1.2, also used in several trials [31,34,35], provides in the current study a similar amount of detected lesions at 2 h p.i. in comparison to 4 h p.i. using a TBR >1.4, however the risk of misclassifying lesions increases. This might also explain the difference between the studies of Nehmeh et al. [34] and Okamoto et al. [36] using [^{18}F]MISO PET imaging in head and neck cancer patients. Nehmeh et al. used a threshold of TBR >1.2 and observed that the measured fractional hypoxic volumes were variable over time. Whereas Okamoto et al. using a threshold of TBR >1.4 found a high reproducibility of tumor hypoxia. In the ideal situation, clinical PET imaging should be correlated with tumor pathological specimens [37], to evaluate the threshold to define tumor hypoxia.

For future dose re-distribution studies it is of importance to gain insight into the spatio-temporal stability of the PET tracer. A rigid registration was performed to compare the [^{18}F]HX4 PET images at 2 h and 4 h p.i. Small errors in the registration can strongly affect the observed correlations negatively [38]. In the current study PET scans were acquired in treatment position reducing the possibility for registration errors. Patients were free-breathing during PET-acquisitions, which might cause a blurring of the PET signal. However, this will not affect the registration, since breathing motion is the same for both acquisitions. By using a careful scan procedure and image registration a good spatio-temporal stability was found.

Limiting the acquisition time is beneficial for practical reasons, to reduce patient movement and to increase patient comfort. As expected, image noise increases when reducing the acquisition time. This results in a significant change in CNR and SUV_{max} for all reduced acquisition times. However TBR_{max} and HF are only significantly influenced when acquisition time is reduced to 5 min. This is in agreement with the results previously showed by Boellaard et al. [39], that SUV_{max} is more sensitive to image noise than SUV ratios like TBR. For this reason SUV_{max} is not the best parameter to evaluate the uptake of hypoxia makers. A trade-off has to be made between image noise and practical issues, nonetheless, the acquisition-time for [^{18}F]HX4 PET imaging at 4 h p.i. should be at least 10 min, with the current administered activity and a modern Time-of-Flight PET/CT scanner. This provides the opportunity to acquire more bed positions, capturing the entire thorax in a 30 min time frame. Another option is to reduce the amount of injected activity, which will have a similar effect on image noise as a reduction of acquisition time.

In conclusion, significant hypoxia was observed in 72% of the NSCLC target lesions (80% of primary tumors and 60% of the involved lymph nodes). The heterogeneous [^{18}F]HX4 uptake pattern was stable between 2 h and 4 h p.i., however the TBR_{max} increased over time, suggesting that imaging at 4 h p.i. is better to reach the highest contrast in [^{18}F]HX4 PET images. [^{18}F]HX4 PET acquisition time can be reduced to 10 min without significant effects on TBR_{max} and HF.

Conflicts of interest

No actual or potential conflicts of interest exist.

Acknowledgments

The authors like to thank the patients who agreed to participate and R. Franssen and C. Urbach from the Department of Nuclear Medicine MUMC for their contribution to the data acquisition. We acknowledge financial support from the CTMM framework (AIRFORCE project), EU 6th and 7th framework program (ARTFORCE and METOXIA program), Interreg (www.eurocat.info), STW (DuCAT), the Kankeronderzoekfonds Limburg from the Health Foundation Limburg and the Dutch Cancer Society (KWF UM 2011-5020, KWF UM 2009-4454, KWF MAC 2011-4970).

Appendix A. Supplementary data

Supplementary data associated with this article can be found, in the online version, at http://dx.doi.org/10.1016/j.radonc.2013.08.031. Preclinical and phase I clinical [^{18}F]HX4 PET/CT images are available at www.cancerdata.org/?q=10.1073/pnas.1102526108 and www.cancerdata.org/?q=10.1007/s00259-010-1437-x

References

[1] van Baardwijk A, Reymen B, Wanders S, et al. Mature results of a phase II trial on individualised accelerated radiotherapy based on normal tissue constraints in concurrent chemo-radiation for stage III non-small cell lung cancer. Eur J Cancer 2012;48:2339–46.
[2] Wouters BG, van den Beucken T, Magagnin MG, Lambin P, Koumenis C. Targeting hypoxia tolerance in cancer. Drug Resist Updat 2004;7:25–40.
[3] Lambin P, van Stiphout RG, Starmans MH, et al. Predicting outcomes in radiation oncology – multifactorial decision support systems. Nat Rev Clin Oncol 2013;10:27–40.
[4] Overgaard J. Hypoxic modification of radiotherapy in squamous cell carcinoma of the head and neck – a systematic review and meta-analysis. Radiother Oncol 2011;100:22–32.
[5] Mortensen LS, Johansen J, Kallehauge J, et al. FAZA PET/CT hypoxia imaging in patients with squamous cell carcinoma of the head and neck treated with radiotherapy: results from the DAHANCA 24 trial. Radiother Oncol 2012;105:14–20.
[6] Eschmann SM, Paulsen F, Reimold M, et al. Prognostic impact of hypoxia imaging with 18F-misonidazole PET in non-small cell lung cancer and head and neck cancer before radiotherapy. J Nucl Med 2005;46:253–60.
[7] Gagel B, Reinartz P, Demirel C, et al. [^{18}F] fluoromisonidazole and [^{18}F] fluorodeoxyglucose positron emission tomography in response evaluation after chemo-/radiotherapy of non-small-cell lung cancer: a feasibility study. BMC Cancer 2006;6:51.
[8] Vera P, Bohn P, Edet-Sanson A, et al. Simultaneous positron emission tomography (PET) assessment of metabolism with (1)(8)F-fluoro-2-deoxy-d-glucose (FDG), proliferation with (1)(8)F-fluoro-thymidine (FLT), and hypoxia with (1)(8)fluoro-misonidazole (F-miso) before and during radiotherapy in patients with non-small-cell lung cancer (NSCLC): a pilot study. Radiother Oncol 2011;98:109–16.
[9] Bittner MI, Wiedenmann N, Bucher S, et al. Exploratory geographical analysis of hypoxic subvolumes using F-MISO-PET imaging in patients with head and neck cancer in the course of primary chemoradiotherapy. Radiother Oncol 2013. epub ahead of print.

[10] Bollineni VR, Kerner GS, Pruim J, et al. PET imaging of tumor hypoxia using 18F-fluoroazomycin arabinoside in stage III–IV non-small cell lung cancer patients. J Nucl Med 2013;54:1–6.
[11] Zips D, Boke S, Kroeber T, et al. Prognostic value of radiobiological hypoxia during fractionated irradiation for local tumor control. Strahlenther Onkol 2011;187:306–10.
[12] Lambin P, Petit SF, Aerts HJ. The E.S.T.R.O. Breur. Lecture from population to voxel-based radiotherapy: exploiting intra-tumour and intra-organ heterogeneity for advanced treatment of non-small cell lung cancer. Radiother Oncol 2009;2010:145–52.
[13] Hendrickson K, Phillips M, Smith W, Peterson L, Krohn K, Rajendran J. Hypoxia imaging with [F-18] FMISO-PET in head and neck cancer: potential for guiding intensity modulated radiation therapy in overcoming hypoxia-induced treatment resistance. Radiother Oncol 2011;101:369–75.
[14] Thorwarth D, Eschmann SM, Paulsen F, Alber M. Hypoxia dose painting by numbers: a planning study. Int J Radiat Oncol Biol Phys 2007;68:291–300.
[15] van Elmpt W, De Ruysscher D, van der Salm A, et al. The PET-boost randomised phase II dose-escalation trial in non-small cell lung cancer. Radiother Oncol 2012;104:67–71.
[16] Bollineni VR, Wiegman EM, Pruim J, Groen HJ, Langendijk JA. Hypoxia imaging using positron emission tomography in non-small cell lung cancer: implications for radiotherapy. Cancer Treat Rev 2012;38:1027–32.
[17] Horsman MR, Mortensen LS, Petersen JB, Busk M, Overgaard J. Imaging hypoxia to improve radiotherapy outcome. Nat Rev Clin Oncol 2012;9:674–87.
[18] Dubois LJ, Lieuwes NG, Janssen MH, et al. Preclinical evaluation and validation of [18F]HX4, a promising hypoxia marker for PET imaging. Proc Natl Acad Sci U S A 2011;108:14620–5.
[19] van Loon J, Janssen MH, Ollers M, et al. PET imaging of hypoxia using [18F]HX4: a phase I trial. Eur J Nucl Med Mol Imaging 2010;37:1663–8.
[20] Doss M, Zhang JJ, Belanger MJ, et al. Biodistribution and radiation dosimetry of the hypoxia marker 18F-HX4 in monkeys and humans determined by using whole-body PET/CT. Nucl Med Commun 2010;31:1016–24.
[21] Chen L, Zhang Z, Kolb HC, Walsh JC, Zhang J, Guan Y. (1)(8)F-HX4 hypoxia imaging with PET/CT in head and neck cancer: a comparison with (1)(8)F-FMISO. Nucl Med Commun 2012;33:1096–102.
[22] Rasey JS, Koh WJ, Evans ML, et al. Quantifying regional hypoxia in human tumors with positron emission tomography of [18F]fluoromisonidazole: a pretherapy study of 37 patients. Int J Radiat Oncol Biol Phys 1996;36:417–28.
[23] Koh WJ, Bergman KS, Rasey JS, et al. Evaluation of oxygenation status during fractionated radiotherapy in human nonsmall cell lung cancers using [F-18]fluoromisonidazole positron emission tomography. Int J Radiat Oncol Biol Phys 1995;33:391–8.
[24] Dubois L, Landuyt W, Haustermans K, et al. Evaluation of hypoxia in an experimental rat tumour model by [(18)F]fluoromisonidazole PET and immunohistochemistry. Br J Cancer 2004;91:1947–54.
[25] Gray AJ, Dische S, Adams GE, Flockhart IR, Foster JL. Clinical testing of the radiosensitiser Ro-07-0582. I. Dose tolerance, serum and tumour concentrations. Clin Radiol 1976;27:151–7.
[26] Saunders ME, Dische S, Anderson P, Flockhart IR. The neurotoxicity of misonidazole and its relationship to dose, half-life and concentration in the serum. Br J Cancer Suppl 1978;3:268–70.
[27] Abolmaali N, Haase R, Koch A, et al. Two or four hour [(1)(8)F]FMISO-PET in HNSCC. When is the contrast best? Nuklearmedizin 2011;50:22–7.
[28] Hu M, Xing L, Mu D, et al. Hypoxia imaging with 18F-fluoroerythronitroimidazole integrated PET/CT and immunohistochemical studies in non-small cell lung cancer. Clin Nucl Med 2013;38:591–6.
[29] Li L, Hu M, Zhu H, Zhao W, Yang G, Yu J. Comparison of 18F-fluoroerythronitroimidazole and 18F-fluorodeoxyglucose positron emission tomography and prognostic value in locally advanced non-small-cell lung cancer. Clin Lung Cancer 2010;11:335–40.
[30] Cherk MH, Foo SS, Poon AM, et al. Lack of correlation of hypoxic cell fraction and angiogenesis with glucose metabolic rate in non-small cell lung cancer assessed by 18F-fluoromisonidazole and 18F-FDG PET. J Nucl Med 2006;47:1921–6.
[31] Trinkaus ME, Blum R, Rischin D, et al. Imaging of hypoxia with (18) F-FAZA PET in patients with locally advanced non-small cell lung cancer treated with definitive chemoradiotherapy. J Med Imaging Radiat Oncol 2013;57:475–81.
[32] Postema EJ, McEwan AJ, Riauka TA, et al. Initial results of hypoxia imaging using 1-alpha-D: -(5-deoxy-5-[18F]-fluoroarabinofuranosyl)-2-nitroimidazole (18F-FAZA). Eur J Nucl Med Mol Imaging 2009;36:1565–73.
[33] Grau C, Overgaard J. Effect of cancer chemotherapy on the hypoxic fraction of a solid tumor measured using a local tumor control assay. Radiother Oncol 1988;13:301–9.
[34] Nehmeh SA, Lee NY, Schroder H, et al. Reproducibility of intratumor distribution of (18)F-fluoromisonidazole in head and neck cancer. Int J Radiat Oncol Biol Phys 2008;70:235–42.
[35] Dirix P, Vandecaveye V, De Keyzer F, Stroobants S, Hermans R, Nuyts S. Dose painting in radiotherapy for head and neck squamous cell carcinoma: value of repeated functional imaging with (18)F-FDG PET, (18)F-fluoromisonidazole PET, diffusion-weighted MRI, and dynamic contrast-enhanced MRI. J Nucl Med 2009;50:1020–7.
[36] Okamoto S, Shiga T, Yasuda K, et al. High reproducibility of tumor hypoxia evaluated by 18F-fluoromisonidazole PET for head and neck cancer. J Nucl Med 2013;54:201–7.
[37] van Baardwijk A, Dooms C, van Suylen RJ, et al. The maximum uptake of (18)F-deoxyglucose on positron emission tomography scan correlates with survival, hypoxia inducible factor-1alpha and GLUT-1 in non-small cell lung cancer. Eur J Cancer 2007;43:1392–8.
[38] Nyflot MJ, Harari PM, Yip S, Perlman SB, Jeraj R. Correlation of PET images of metabolism, proliferation and hypoxia to characterize tumor phenotype in patients with cancer of the oropharynx. Radiother Oncol 2012;105:36–40.
[39] Boellaard R, Krak NC, Hoekstra OS, Lammertsma AA. Effects of noise, image resolution, and ROI definition on the accuracy of standard uptake values: a simulation study. J Nucl Med 2004;45:1519–27.